Journal of *Marine Science and Engineering*

MDPI

Article

Data-Driven Load Suppression and Platform Motion Optimization for Semi-Submersible Wind Turbines

Liqing Liao [1], Qian Huang [1], Li Wang [1,*], Jian Yang [1], Dongran Song [1], Sifan Chen [2] and Lingxiang Huang [3,4]

[1] School of Automation, Central South University, Changsha 410083, China; zdh-dqkz@csu.edu.cn (L.L.); tomhuangq@163.com (Q.H.); jian.yang@csu.edu.cn (J.Y.); songdongran@csu.edu.cn (D.S.)
[2] Mingyang Smart Energy Group Co., Ltd., Zhongshan 528437, China; chensifan@mywind.com.cn
[3] College of Electrical and Information Engineering, Hunan University, Changsha 410083, China; huanglingxiang@hewp.com.cn
[4] State Key Laboratory of Offshore Wind Power Equipment and Wind Energy High-Efficient Utilization, Xiangtan 411100, China
* Correspondence: 224601008@csu.edu.cn

Abstract

To address the issues of large fatigue loads on key components and poor platform motion stability under the coupling effect of wind, waves, and internal excitations in semi-submersible wind turbines, this paper proposes a data-driven load suppression and platform motion optimization method. First, the NREL 5 MW OC4 semi-submersible wind turbine is used as the research object. Wind-wave environment and aeroelastic simulation models are constructed based on TurbSim and OpenFAST. The rainflow counting method and Palmgren–Miner rule are applied to calculate the damage equivalent load (DEL) of key components, and the platform's maximum horizontal displacement (Smax) is defined to represent the motion range. Secondly, a systematic analysis is conducted to examine the effects of servo control variables such as generator speed, yaw angle, and active power on the DELs of the blade root, tower base, drivetrain, mooring cables, and platform Smax. It is found that the generator speed and the yaw angle have significant impacts, with the DELs of the blade root and drivetrain showing a strong positive correlation with Smax. On this basis, a fatigue load model based on random forests is established. A multi-objective optimization framework is built using the NSGA-II algorithm, with the objectives of minimizing the total DEL of key components and Smax, thereby optimizing the servo control parameters. Case studies based on actual marine environmental data from the East China Sea show that, compared to the baseline configuration (a typical unoptimized control strategy), the optimization results lead to a maximum reduction of 14.1% in the total DEL of key components and a maximum reduction of 16.95% in Smax. The study verifies the effectiveness of data-driven modeling and multi-objective optimization for coordinated control, providing technical support for improving the structural safety and operational stability of semi-submersible wind turbines.

Keywords: semi-submersible wind turbine; fatigue load; data-driven; platform motion optimization; multi-objective optimization

check for updates

Academic Editor: Atilla Incecik

Received: 21 August 2025
Revised: 11 September 2025
Accepted: 12 September 2025
Published: 23 September 2025

Citation: Liao, L.; Huang, Q.; Wang, L.; Yang, J.; Song, D.; Chen, S.; Huang, L. Data-Driven Load Suppression and Platform Motion Optimization for Semi-Submersible Wind Turbines. *J. Mar. Sci. Eng.* **2025**, *13*, 1839. https://doi.org/10.3390/jmse13101839

Copyright: © 2025 by the authors. Licensee MDPI, Basel, Switzerland. This article is an open access article distributed under the terms and conditions of the Creative Commons Attribution (CC BY) license (https://creativecommons.org/licenses/by/4.0/).

1. Introduction

With the increasing consumption of fossil fuels and global climate warming, the development of green renewable energy has become a consensus, and the global installed capacity of offshore wind energy is rapidly growing [1]. Semi-submersible wind turbines,

subjected to both external excitations such as wind and waves, and internal excitations from rotor rotation, experience complex structural vibrations. This results in large fatigue loads on key components, significantly impacting structural reliability and operational safety [2]. In recent years, advancements in related technologies have been made. Coupled dynamic analysis, fatigue load modeling, and platform motion optimization methods have gradually been improved. Demonstration projects such as Hywind Scotland (2017) [3], WindFloat Atlantic (2019) [4], and the "Three Gorges Leading" (2021) [5] have verified the practical feasibility of semi-submersible wind turbines, but optimizing fatigue loads and platform motion remains a multi-disciplinary challenge.

Due to the unique structural and dynamic characteristics of semi-submersible wind turbines, traditional pitch control strategies are not suitable [6]. Researchers have proposed a series of new control strategies and frameworks. One of the most representative innovative methods is the independent pitch control. This method not only optimizes the response performance of the wind turbine, but also significantly reduces the stress on key structural components such as the tower and blades, thereby lowering their fatigue loads and improving the safety and long-term reliability of wind turbines in complex environments [7]. In recent years, independent pitch control has been extensively studied in the servo control of semi-submersible wind turbines. Bai et al. [6] designed an independent pitch control method based on an equivalent wind speed model, addressing the limitations of traditional collective pitch control in semi-submersible wind turbines. Gong et al. [8] proposed a new adaptive nonlinear pitch controller aimed at balancing power generation and reducing platform motion. Although independent pitch control can reduce loads to some extent, its effectiveness still has certain limitations.

To achieve integrated optimization of load suppression and platform motion, researchers have attempted to optimize both pitch and yaw controllers simultaneously. Han et al. [9] proposed using a static feedforward controller combined with generator speed feedback to adjust the nacelle yaw angle and rotor blade pitch angle, passively utilizing aerodynamics to achieve load optimization. Qi et al. [10] proposed an overlay proportional model-free adaptive control, optimizing the rotor speed and yaw motion of the semi-submersible wind turbine to address the effects of rotor aerodynamics and platform motion coupling. Stewart et al. [11] applied a genetic algorithm to integrate the floating platform model into the optimization function, achieving a globally optimal design of a tuned mass damper, which successfully reduced fatigue damage to the tower. Xie et al. [12] proposed a new reinforcement learning-based control scheme, combining independent and collective pitch control to balance two key objectives: load reduction and power regulation. Lara et al. [13] used a multi-objective genetic optimization algorithm to determine the optimal adaptive generator torque control parameters based on wind speed and wave height, with the goal of minimizing fatigue loads on the tower and low-speed shaft and reducing power fluctuations. This strategy effectively reduced fatigue loads on the transverse tower, but at the cost of increased power signal oscillations and low-speed shaft fatigue. Zhou et al. [14] established a data-driven model for key component loads and platform motion degrees of freedom of semi-submersible wind turbines based on Kriging models, using the NSGA-II algorithm for long-term dynamic iterative optimization to achieve a long-term dynamic optimization-based evaluation method. The above results fully demonstrated the effectiveness of joint optimization of load suppression and platform motion, but they have not sufficiently considered modeling and optimization with key operational parameters such as rotor speed, power, and yaw angle as input. In addition to control-oriented approaches, extensive research has addressed condition monitoring and structural health monitoring (SHM) of wind turbines and offshore structures. For instance, recent reviews have summarized two decades of non-destructive SHM techniques

for wind turbines, including vibration-based methods, acoustic emission, ultrasonic testing, and advanced signal processing [15]. Comparable progress has been made for offshore structures, where data-driven and statistical methods, such as cointegration strategies, have been applied to assess damage under combined wind and wave excitations [16]. These studies underscore the importance of integrating monitoring data with advanced analytics for safety assurance. However, most existing SHM research focuses on fault detection or damage identification, with relatively less attention on linking monitoring insights to real-time turbine control optimization.

The rapid growth of offshore wind energy, particularly semi-submersible floating wind turbines, has highlighted the need for improving their structural reliability and operational stability. While previous studies have focused on control optimization or structural health monitoring independently, few have integrated them for real-time optimization in the context of floating wind turbines. This study aims to fill this gap by proposing a data-driven approach for optimizing both fatigue loads and platform motion, with the ultimate goal of enhancing the performance of semi-submersible wind turbines under variable marine conditions. First, the NREL 5 MW OC4 semi-submersible wind turbine (National Renewable Energy Laboratory, USA) is used as the research object. Wind-wave environment and aeroelastic simulation models are constructed based on TurbSim (version: v2.00, https://www.nrel.gov/wind/nwtc/turbsim, accessed on 11 September 2025) and OpenFAST (version: v4.1.1, https://github.com/OpenFAST/openfast, accessed on 11 September 2025). The rainflow counting method and Palmgren–Miner rule are applied to calculate the damage equivalent load (DEL) of key components, and the platform's maximum horizontal displacement (Smax) is defined to represent the motion range. Secondly, an in-depth analysis is performed to examine the effects of servo control parameters such as the generator speed, the yaw angle, and the active power on the DELs of the blade root, tower base, drivetrain, mooring cables, and platform Smax. Based on this, a fatigue load data-driven model based on random forests is established, and a multi-objective optimization framework is built using the NSGA-II algorithm, with the goal of minimizing the total DEL of key components and Smax, thereby optimizing the servo control parameters. Finally, case studies based on actual marine environment data from the East China Sea are conducted. Compared with existing references, the present study makes three distinctive contributions.

(1) Instead of treating pitch or torque as isolated variables, we systematically incorporate generator speed, yaw angle, and active power as integrated servo control parameters, providing a more comprehensive representation of the coupled load–motion relationship.
(2) Unlike reinforcement learning-based pitch/yaw control, and adaptive torque/pitch strategies, we propose a comprehensive optimization framework for fatigue load and platform motion of the semi-submersible wind turbine, which is fully data-driven using integrated servo control parameters.
(3) By embedding this high-fidelity data-driven model into an NSGA-II multi-objective optimization framework, we demonstrate simultaneous reductions of up to 14.1% in key component fatigue loads and 16.95% in platform motion—a level of coordinated performance improvement not explicitly achieved in prior literature. These innovations highlight the novelty and practical value of the proposed method for improving the structural safety and operational stability of semi-submersible wind turbines.

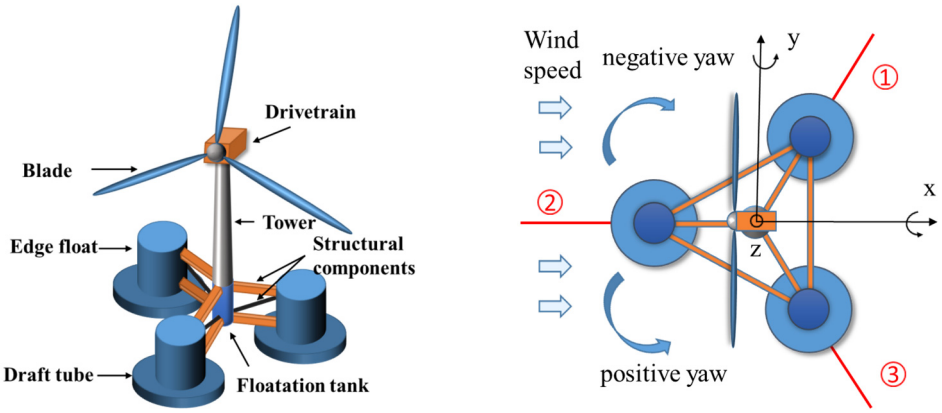
2. Preliminary Knowledge

The fatigue loads of semi-submersible wind turbines are affected by various control parameters, including the generator speed, the yaw angle, and the active power. Focusing on influencing factors, this section firstly introduces the semi-submersible wind turbine

model, wind–wave environment generation, and servo control model. Subsequently, the methods of calculating the fatigue load and the platform motion range are explained.

2.1. Semi-Submersible Wind Turbine Model

To provide a realistic and widely recognized research object, this study selects the NREL 5 MW OC4 semi-submersible (National Renewable Energy Laboratory, USA) wind turbine as the target system [17]. Its structure is shown in Figure 1, with the main turbine parameters listed in Table 1 and the floating platform characteristics summarized in Table 2. This baseline model offers a representative platform for subsequent environmental simulation, control modeling, and optimization analysis.



(**a**) (**b**)

Figure 1. The overall structure of the NREL 5 MW OC4 semi-submersible offshore wind turbine. (**a**) The structure of the semi-submersible offshore wind turbine; (**b**) arrangement of mooring system structure.

Table 1. Key parameters of the baseline NREL 5 MW wind turbine.

Attributes	Description
Rated Power	5 MW
Rated Speed	1173.7 rpm
Turbine Type	Upwind, Three Blades
Control Method	Variable speed control, collective pitch control
Rotor and Hub Diameter	126 m, 3 m
Hub Height	90 m
Cut-in, Rated, and Cut-out Wind Speeds	3 m/s, 11.4 m/s, 25 m/s
Cut-in, Rated Speeds	6.9 rpm, 12.1 rpm

Table 2. OC4 semi-submersible floating system parameters.

Attributes	Description
Platform Type	Tri-Float Semi-Submersible
Working Water Depth	200 m
Mooring Line Type	Catenary, 120° Symmetrical Distribution
Platform Foundation Depth Below SWL	20 m
Platform Mass	1.3473×10^7 kg
Displacement	13,917 m^3

2.2. Wind–Wave Environment Generation

The operational environment of semi-submersible wind turbines is dominated by wind, waves, and currents, which must be realistically generated to evaluate structural

responses. TurbSim [18,19] is used to generate full-field three-dimensional turbulent wind, with a duration of 800 s. To meet IEC requirements for short-term damage equivalent load calculation [20], only the last 600 s are retained to avoid initialization effects. In addition to wind and turbulence, the marine environment also includes waves and currents. These are modeled in OpenFAST [21], where InflowWind and HydroDyn define external conditions, and the resulting loads are coupled with the turbine through ServoDyn, ElastoDyn, and MoorDyn. This setup enables aero-hydro-servo-elastic simulations of the NREL 5 MW OC4 semi-submersible wind turbine, producing time-series data of structural bending moments and platform motions for subsequent fatigue load analysis. The resulting aerodynamic and hydrodynamic conditions provide the necessary inputs for fatigue load calculation and platform motion assessment. TurbSim and OpenFAST not only provide open-source accessibility and high-fidelity modeling of turbulent inflow and coupled aero-hydro-servo-elastic dynamics, but also ensure seamless compatibility with the NREL 5 MW OC4 reference turbine. This makes them particularly well-suited to the objectives of this study, which require accurate simulation of fatigue loads and platform motions under realistic marine environments.

2.3. Servo Control Model

After generating the wind–wave environment, a servo control model is established to operate the semi-submersible wind turbine. The aerodynamic power is determined by the power coefficient $C_P(\lambda, \beta)$, where the tip-speed ratio λ and pitch angle β correspond to torque and pitch control, respectively [22]. The aerodynamic coefficient C_P of the NREL 5 MW wind turbine is shown in Figure 2. In addition, the yaw angle φ can adjust the captured power by altering the inflow condition. As shown in Figure 3, different combinations of ω_g, β, and φ may yield the same power output but result in different component loads and platform motions. To systematically evaluate these effects, an external control system is implemented in Matlab/Simulink (version: R2022b, https://www.mathworks.com/help/install/ug/install-products-with-internet-connection.html, accessed on 11 September 2025) and coupled with OpenFAST [23] for aeroelastic simulations. The control strategy includes: (i) adjusting pitch through a PI controller to track the reference generator speed; (ii) regulating active power via the torque controller; and (iii) applying different yaw angles through the ElastoDyn module to investigate their impact on fatigue loads and platform motion.

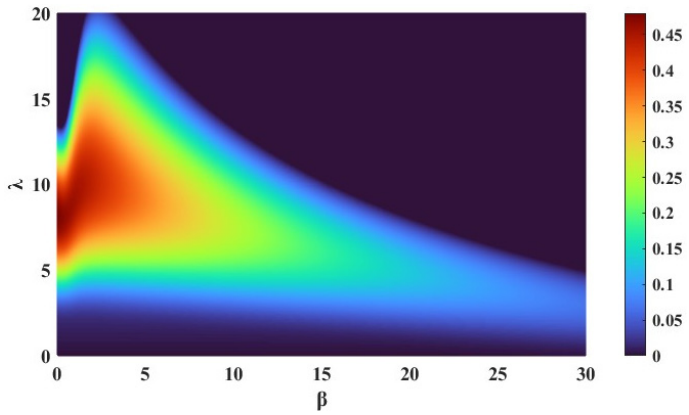


Figure 2. Aerodynamic coefficient C_P (λ, β) of the NREL 5 MW wind turbine.

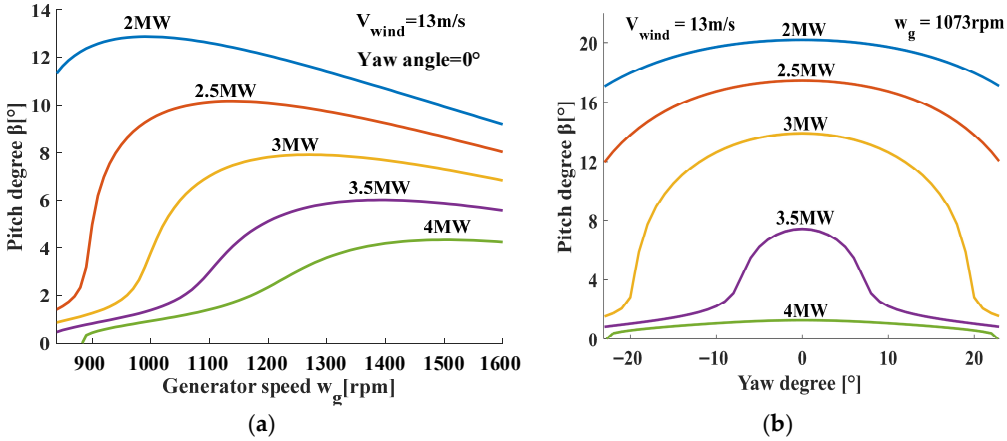


Figure 3. Curves of the control variables of the wind turbine servo mechanism under different power conditions. (**a**) The relationship between pitch angle and generator rotational speed (rpm), (**b**) The relationship between pitch angle and yaw angle (°).

2.4. Framework for Fatigue Load Modeling of Floating Wind Turbines

To quantitatively link operating conditions with fatigue damage, a standardized procedure for fatigue load calculation is established. The rainflow counting method [24] and the Palmgren–Miner rule [25] are applied to compute the damage equivalent load (DEL) of blades, tower, drivetrain, and mooring cables. In addition, the maximum horizontal displacement is used to characterize platform motion.

The steps for calculating the damage equivalent load are as follows: first, the rainflow counting method [26] is used to decompose fluctuating loads into individual hysteresis cycles by counting the local peaks and valleys; then, based on the number of fatigue cycles and the Palmgren–Miner rule, the damage equivalent load is calculated to represent the equivalent fatigue load generated under constant load mean and frequency conditions. The formula is as follows [27,28]:

$$DEL_j^{ST} = \left(\frac{\sum_i \left(n_{ji} \left(L_{ji}^R \right)^m \right)}{n_j^{STeq}} \right)^{\frac{1}{m}} \tag{1}$$

$$n_j^{STeq} = f^{eq} T_j \tag{2}$$

where f^{eq} is the frequency of the damage equivalent load; T_j is the time of time series j; n_j^{STeq} is the total equivalent fatigue count for time series j; n_{ji} is the damage count for load cycle i and time series j; n_{ji} is the range for load cycle iii and time series j; m is the Wöhler exponent, with values of 3, 4, and 5 for the tower, LSS, and mooring lines, respectively, and 8, 10, and 12 for the blades; DEL_j^{ST} is the short-term DEL for time series j with fixed mean load.

In this study, MLife (version: v1.01.00a_0, https://www.nrel.gov/wind/nwtc/mlife, accessed on 11 September 2025) software is employed for fatigue load post-processing, capable of directly handling OpenFAST output results and performing fatigue analysis compliant with IEC standards. This ensures a reliable and standardized assessment of component loading. Table 3 lists the mechanical bending moment elements selected for fatigue post-processing and their brief descriptions. The analyzed fatigue moments include the two bending moments at the root of the blade (out-of-plane moment and flapwise moment), the two bending moments at the tower base (lateral moment and fore-aft moment), and the two bending moments at the LSS (rotational y-axis moment and rotational z-axis moment). Additionally, the tension of the three mooring lines at the anchor

points is analyzed for fatigue. These elements are critical performance indicators when evaluating a semi-submersible wind turbine system [7], reflecting the most important mechanical torques in the core components of the semi-submersible wind turbine (tower, LSS, blades, and mooring lines).

Table 3. Component elements selected for fatigue post-processing (their abbreviations taken from OpenFAST).

Name	Description	Unit
RootMxb1	Out-of-plane bending moment at the blade root	[kN m]
RootMyb1	Flapwise bending moment at the blade root	[kN m]
LSSGagMya	Rotational y-axis moment at the drivetrain	[kN m]
LSSGagMza	Rotational z-axis moment at the drivetrain	[kN m]
TwrBsMxt	Lateral (or roll) moment at the tower base	[kN m]
TwrBsMyt	Fore-aft (or pitch) moment at the tower base	[kN m]
ANCHTEN1	Tension at anchor 1	[N]
ANCHTEN2	Tension at anchor 2	[N]
ANCHTEN3	Tension at anchor 3	[N]

Furthermore, the floating platform motion includes six degrees of freedom, including surge, sway, heave, roll, pitch, and yaw, as shown in Figure 1b. Since the heave and pitch responses of semi-submersible platforms are relatively small [8,29], this study focuses on analyzing the platform motion range in the surge and sway directions, which represent the horizontal motion range.

In dynamic analysis, the horizontal displacement of floating wind turbines, relative to the initial platform location, is more suitable to describe the platform's motion compared to considering surge and sway independently. The maximum displacement is usually a design constraint for the mooring system. By calculating the vector sum of the surge and the sway directions, the displacement of the floating wind turbine can be obtained [9]. Therefore, the maximum horizontal displacement is used to measure the platform motion range. The simplified formula of calculating the horizontal displacement is as follows:

$$\vec{S} = \vec{X} + \vec{Y} \tag{3}$$

where $\vec{S}$ is the horizontal displacement of the platform; $\vec{X}$ is the surge motion of the platform; $\vec{Y}$ is the sway motion of the platform.

Thus, the maximum horizontal displacement is calculated as follows:

$$\vec{S}_{max} = MAX(\vec{S}_{200}, \vec{S}_{0.0125}, \cdots, \vec{S}_t, \cdots, \vec{S}_{800}) \tag{4}$$

where $\vec{S}_{max}$ is the maximum horizontal displacement and $\vec{S}_t$ is the horizontal displacement at time t, which is 0.0125 s in this study.

3. Influence of Control Variables on the DEL of Key Components

The objective of this section is to analyze the fatigue loads and platform motion of key components in a semi-submersible wind turbine under different control variables. To achieve this, the fatigue loads and the platform motion of key parts of the semi-submersible wind turbine (including root of the blade, tower base, drivetrain, and mooring lines) are analyzed under various conditions with different generator speeds, yaw angles, and active power. Based on these analyses, a correlation analysis is conducted, exploring the relationship between the components' fatigue loads and the platform motion of the semi-submersible wind turbine.

3.1. Acquisition of DEL Data for Key Components

Figure 4 shows the overall diagram of the simulation experiment. To check the structural response of the semi-submersible floating turbine under different control variables, free wind vectors are generated by TurbSim and used as input. Then, the external controller in Matlab/Simulink implements the servo control, followed by OpenFAST to compute the signals of the fatigue loads and the platform motion for the time series. Finally, MLife is used to obtain the DEL for the four key components and to calculate the maximum horizontal platform displacement $\vec{S}_{max}$.

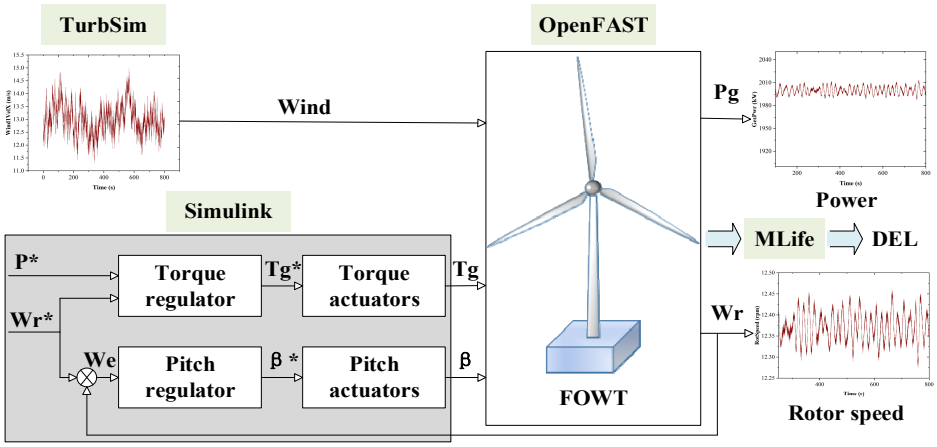


Figure 4. Overall block diagram of the simulation experiment. ("*" indicates target or expected value).

To investigate the effects of operating conditions on DEL and Smax under different output power levels, a combination of the generator speed, the yaw angle, and the active power settings was performed. The input parameters for the simulation model are summarized in Table 4, where 30 different NTM wind speed seeds are simulated and post-processed for each input combination (ω_{gset}, P_{set}^{WT}) and (φ_{gset}, P_{set}^{WT}) with a turbulence intensity of 5%.

Table 4. Simulation parameter settings.

Parameters	Range	Freedom Degrees
Wind Speed V	13 m/s	1
Turbulence Intensity	5%	1
Active Power P_{set}^{WT}	2 MW:0.25 MW:4.25 MW	10
Generator Speed ω_{gset}	973 rpm, 1073 rpm, 1173 rpm	3
Yaw Angle φ_{gset}	$-20°$, $-10°$, $0°$, $10°$, $20°$	5
Experiment Runs	30	30

(1) Settings of Generator Speed: different generator speeds under power-limiting mode on platform motion and DEL are set by following the operational trajectory curves of the wind turbine at different active powers, corresponding to the pitch angle and generator speed, selected from Figure 3a. The generator speeds are set to 973 rpm, 1073 rpm, and 1173 rpm for active power regulation, with the yaw angle fixed at 0° for all settings.

(2) Settings of Yaw Angle: different yaw angles under power-limiting mode on platform motion and DEL are set by following the operational trajectory curves corresponding to the pitch angle and yaw angle for various active powers selected from Figure 3b. Positive yaw angles (10° and 20°), negative yaw angles (−10° and −20°), and no yaw

(0°) were chosen for the five yaw operation conditions. The generator speed is set to 1073 rpm, following the active power control strategy.

(3) Settings of Active Power: different active power outputs are set under power-limiting mode on the platform motion and DEL. Considering that the generator should operate at or below the rated torque, the wind turbine active power output is set between 2 MW and 4.25 MW, with increments of 0.25 MW.

3.2. Analysis of Fatigue Load and Platform Motion

After obtaining the DEL data for key components, the influence of different generator speeds and yaw angles on the damage equivalent loads of the key components, platform motion trajectories, and maximum horizontal platform displacement was analyzed [30]. Figures 5 and 6 show the results of the maximum horizontal platform displacement and key component DEL under different control parameters. Based on these two figures, the following conclusions can be drawn:

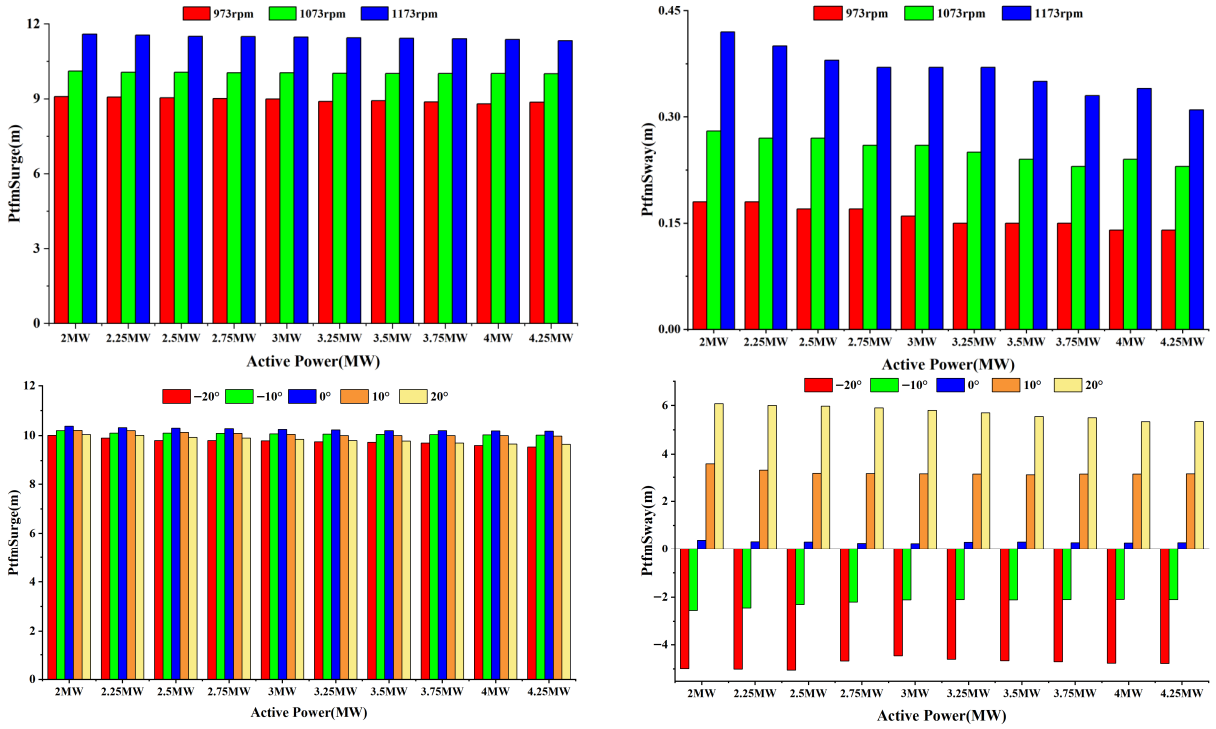


Figure 5. Maximum horizontal offset of the floating wind turbine platform under different control parameters.

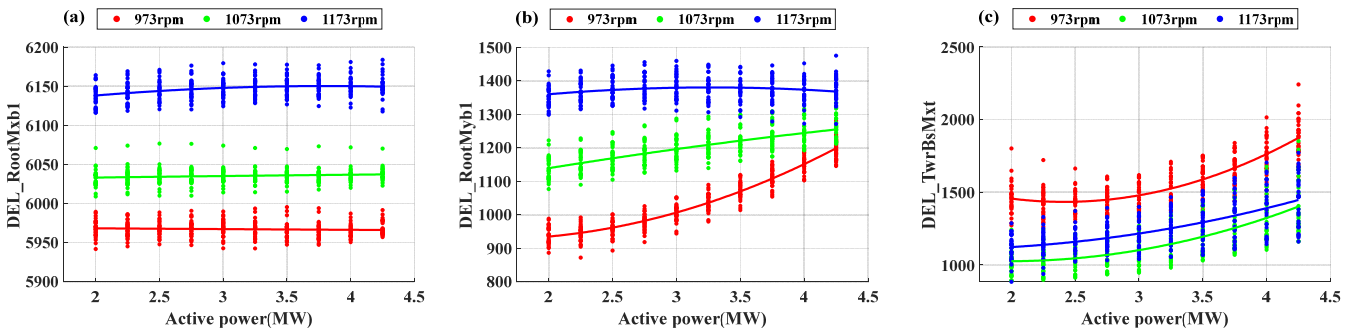


Figure 6. *Cont.*

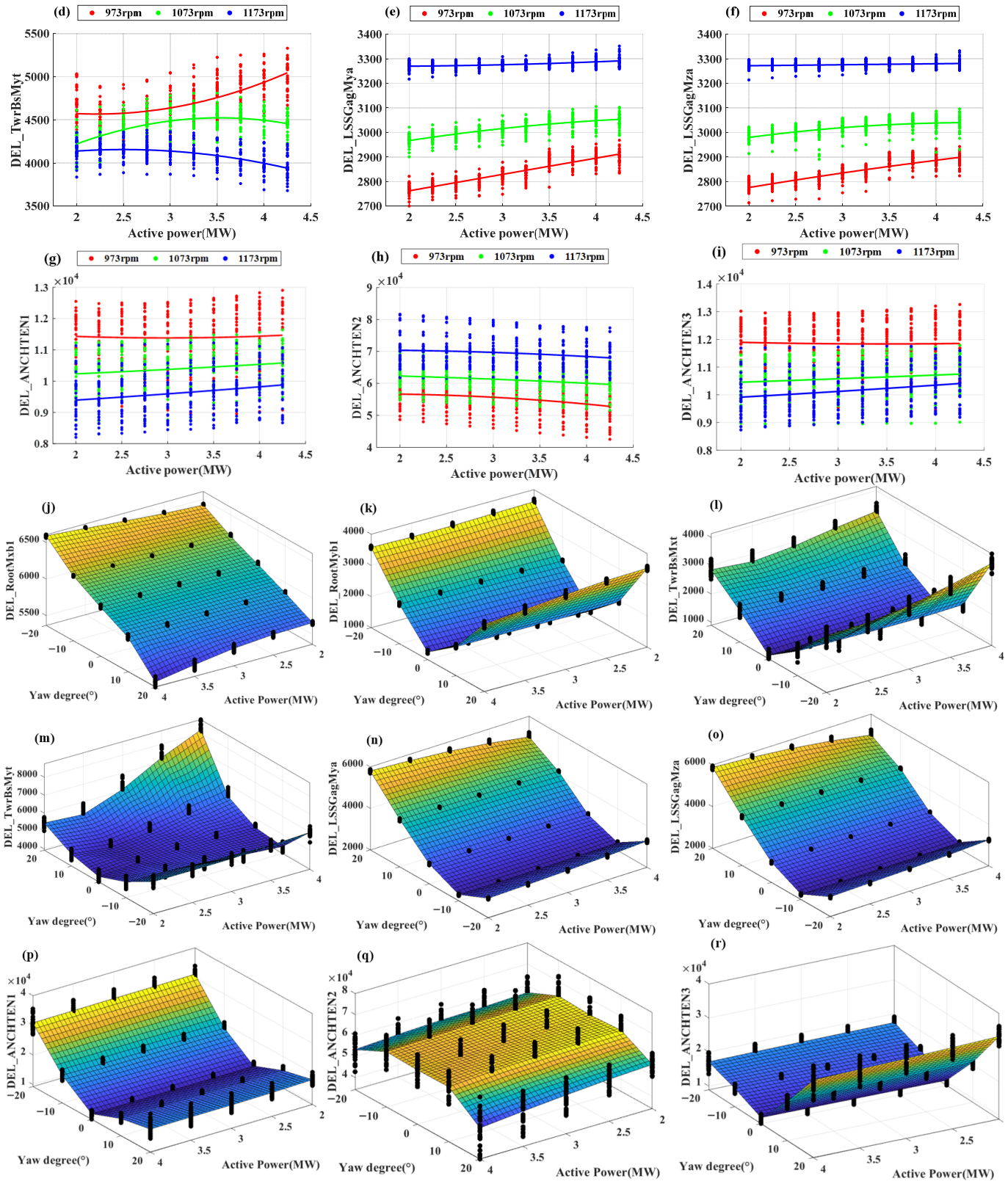


Figure 6. DEL of key components of the floating wind turbine under different control parameters. (**a**–**i**): Scatter plots and regression lines of the DEL at the blade root (**a**,**b**), tower base (**c**,**d**), drivetrain (**e**,**f**), and three mooring anchor points (**g**–**i**) under different generator speeds and active power; (**j**–**r**): Scatter plots and regression surfaces of the DEL at the blade root (**j**,**k**), tower base (**l**,**m**), drivetrain (**n**,**o**), and three mooring anchor points (**p**–**r**) under different yaw angles and active power.

(1) Generator speed significantly affects fatigue load of wind turbine components: when increasing the generator speed, the fatigue loads on the blade root out-of-plane moment and flapwise moment, as well as the rotational moments in both directions of the drivetrain, increase significantly. By comparison, the fatigue load on the fore-aft and lateral moments of tower base decreases. Additionally, due to the increase in generator speed, the platform experiences a displacement in the surge positive direction. As a result, the fatigue loads on the first and third mooring lines decrease, and the fatigue loads on the second mooring line go higher.

(2) Yaw angle significantly affects fatigue load of wind turbine components: positive and negative yaw increase the fatigue loads of the blade root flapwise moment, but the blade root out-of-plane moment monotonically decreases with yaw displacement. Yaw action also induces larger lateral aerodynamic loads, which increase the fatigue loads on the fore-aft and lateral moments of the tower base. For the drivetrain, effective yaw is observed in the negative yaw direction. Furthermore, yaw causes a change in the forces on the three mooring lines due to the generated crosswind load. Since the first and third mooring lines are symmetrically placed along the inflow wind direction, their fatigue loads exhibit symmetry under different yaw actions.

(3) Active power has a significant impact on fatigue load of blade root, tower base, and drivetrain, but a smaller impact on mooring lines: When there is no yaw, an increase in active power significantly induces the fatigue loads of the blade root flapwise moment and the two rotational moments of the drivetrain at low generator speeds. Meanwhile, the fatigue loads of the tower base fore-aft and lateral moments are more sensitive to active power changes. When yaw is introduced, the impact of active power changes on the blade root flapwise moment decreases, but the tower base fore-aft moment remains highly sensitive to it. Additionally, under positive yaw, at high active power, the loads for the two rotational moments of the drivetrain slightly decreases. However, the impact of yaw and non-yaw conditions on the fatigue load of the mooring lines remains relatively small.

(4) Generator speed and yaw angle increase the platform motion range, while active power has a smaller impact: When only increasing the generator speed, for every 100 rpm, the steady-state point in the surge direction moves approximately 1 m further. When the generator speed remains constant and only the yaw angle is changed, for every 10° change in yaw, the movement distance along the sway direction increases by about 2 m, and the trajectory of the platform motion shifts towards the yaw diagonal direction. In contrast, when only changing the active power from 2 MW to 4.25 MW, under different yaw conditions, it results in a maximum reduction of about 0.46 m in the steady-state displacement along the surge direction, indicating a much smaller variation.

4. Comprehensive Optimization of Fatigue Loads and Platform Motion for Semi-Submersible Wind Turbine

As shown in Figure 7, the comprehensive optimization framework for fatigue load and platform motion of the semi-submersible wind turbine consists of three main stages: data preparation and analysis, multi-objective optimization with data-driven modeling, optimization scheme analysis and comparison.

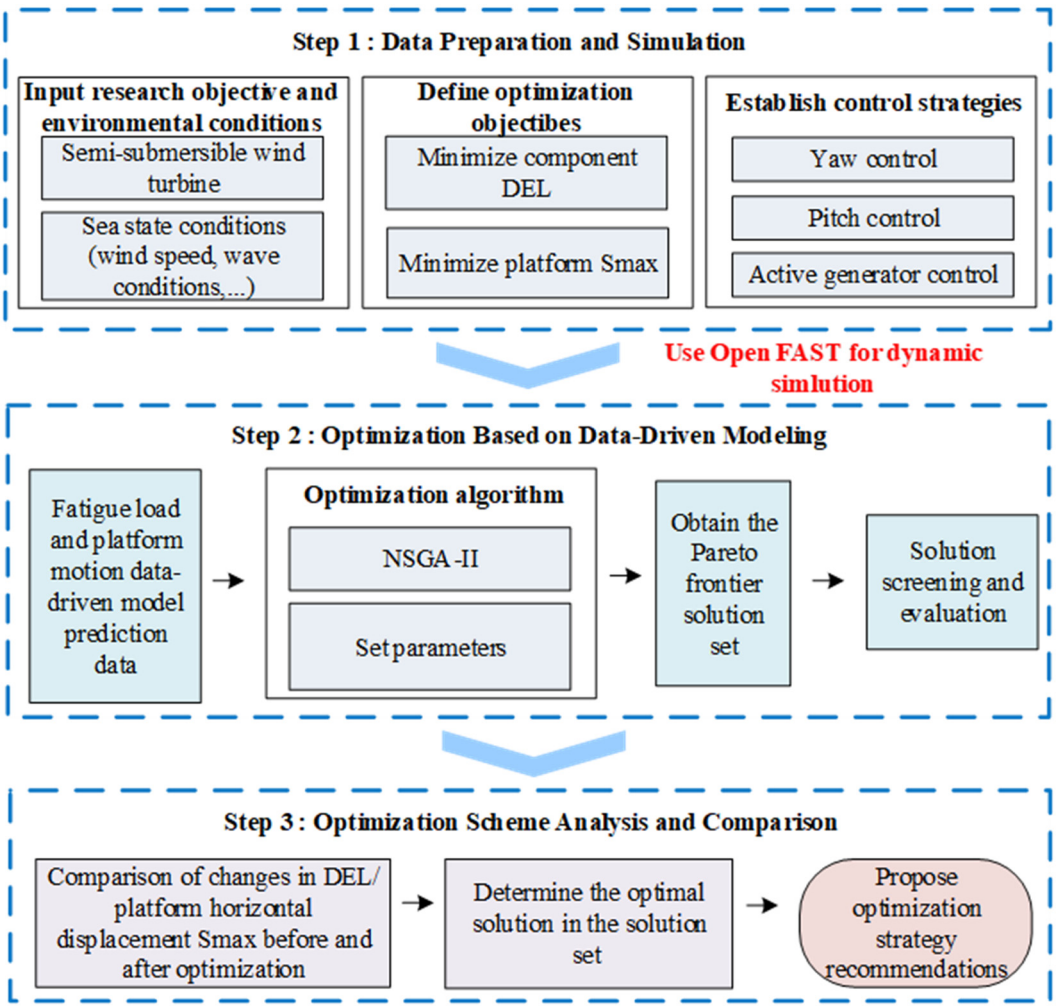


Figure 7. Comprehensive optimization for fatigue loads and platform motion of semi-submersible wind turbines.

4.1. Data-Driven Modeling of DEL for Key Components

As shown in Figure 8, the process for modeling the fatigue load of the floating wind turbine includes four main stages. For details, please refer to [31].

(1) Establishing a joint probability distribution model for wind and wave parameters: The Maximum Likelihood Method is used to determine the marginal distribution parameters for each wind and wave parameter. The goodness-of-fit is evaluated using AIC, BIC, and RMSE. This establishes the marginal distributions for the wind and wave parameters. Then, a Bayesian framework with a residual-based Gaussian likelihood function is used to estimate the parameters of the two-dimensional copula function. The goodness-of-fit is assessed with AIC, and the optimal copula function is determined. Finally, the C-Vine copula theory is applied to establish a joint probability distribution model for four-dimensional random variables (wind speed, wave height, wave period, and wind direction).

(2) Monte Carlo sampling to obtain representative sample conditions: After constructing the joint PDF of the marine environmental variables, the Monte Carlo sampling method is used to obtain representative sample conditions for the four variables (wind speed x_1, wave height x_2, wave period x_3, and wind direction x_4), which serve as the environmental input conditions for subsequent simulation modeling.

(3) FAST simulation sampling conditions: To build a fatigue load data-driven model for the key components (blade root and tower base), a large amount of valid data is required to create the database. After determining the representative load conditions, OpenFAST is used to simulate fatigue loads for all sampled conditions.

(4) Machine learning-based damage equivalent load modeling: Machine learning is used to build the fatigue load model. The model inputs include environmental variables (wind speed, wave height, wave period, wind direction) and operational state variables (rotor speed, yaw angle, and pitch angle). The outputs are the damage equivalent load values for six bending moments at the blade root (RootMxb1, RootMyb1, RootMzb1) and tower base (TwrBsMxt, TwrBsMyt, TwrBsMzt).

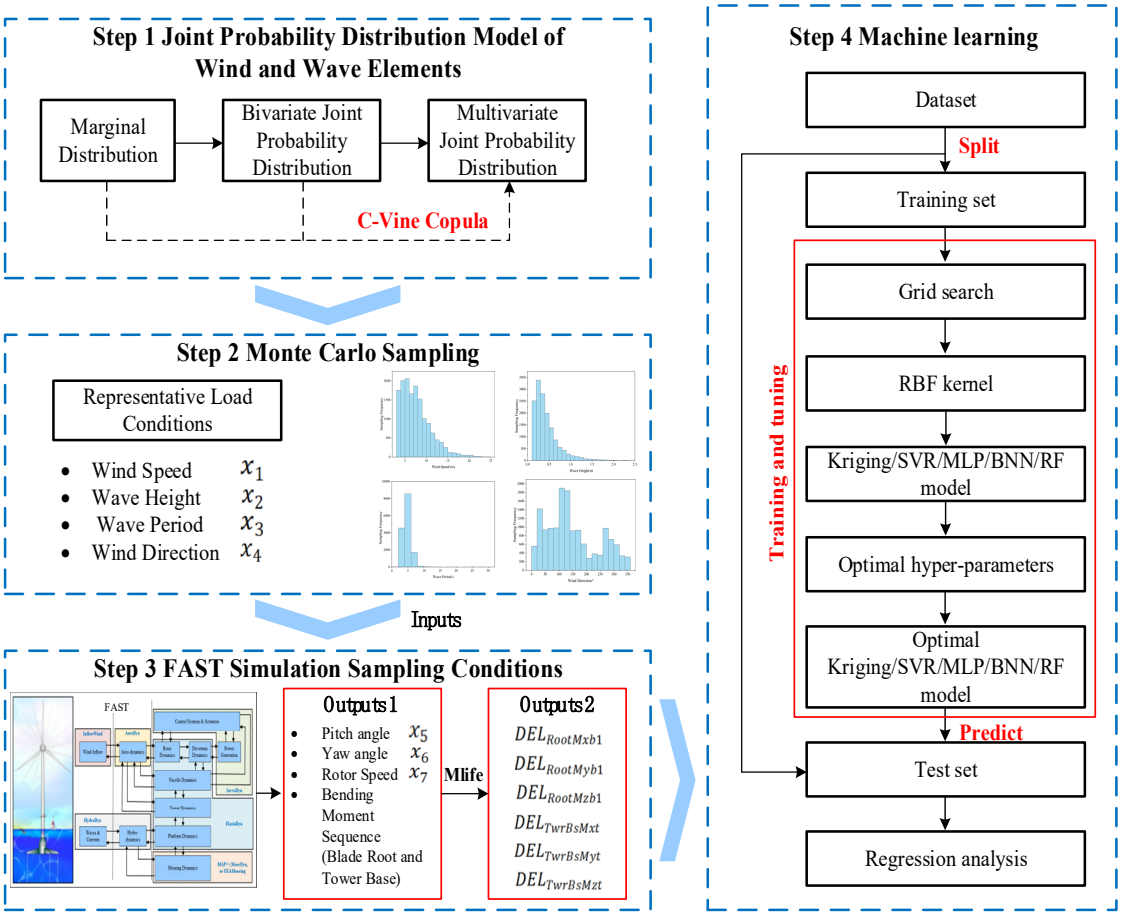


Figure 8. Framework of the proposed load modeling method for floating wind turbines.

Table 5 shows the overall prediction error results (MSE and RMSE) for the six bending moment DEL values using the five machine learning models and the traditional polynomial regression model. It is clearly observed that, overall, the RF, Kriging, and SVR models perform better, while the MLP and BNN models have relatively higher prediction errors, and the polynomial regression model has the highest prediction error. Compared to the five machine learning models, the traditional polynomial regression model generally has an overall error value greater than 1, indicating larger prediction errors. Among the five machine learning models, the RF model consistently exhibits an overall prediction error of less than 0.05 for all six bending moment DELs, with the smallest overall error reaching 0.0021. This indicates that the RF model performs best in predicting the fatigue loads at the blade root and tower base of the semi-submersible wind turbine and is the best choice for establishing the prediction model for the bending moment DELs at the blade root and tower base.

Table 5. Overall error values of five machine learning models and polynomial regression models.

Bending Moment	MSE					
	Kriging	MLP	SVR	BNN	RF	PR
RootMxb1	0.0055	0.2593	0.0388	0.1192	0.0021	1.1094
RootMyb1	0.0177	0.1003	0.0311	0.2377	0.0132	1.3507
RootMzb1	0.0619	0.1726	0.0334	0.1093	0.0232	5.7964
TwrBsMxt	0.0166	0.1186	0.0440	0.3939	0.0126	3.6024
TwrBsMyt	0.0619	0.1168	0.0557	0.1014	0.0390	1.0022
TwrBsMzt	0.0293	0.2304	0.0218	0.1259	0.0117	1.6781
Bending Moment	**RMSE**					
	Kriging	**MLP**	**SVR**	**BNN**	**RF**	**PR**
RootMxb1	0.0741	0.5092	0.1969	0.3452	0.0458	1.0532
RootMyb1	0.1330	0.3167	0.1763	0.4875	0.1148	1.1621
RootMzb1	0.2487	0.4154	0.1827	0.3306	0.1523	2.4075
TwrBsMxt	0.1288	0.3443	0.2097	0.6276	0.1122	1.8979
TwrBsMyt	0.2487	0.3417	0.2360	0.3184	0.1974	1.0010
TwrBsMzt	0.1711	0.4800	0.1476	0.3548	0.1081	1.2954

4.2. Multi-Objective Optimization Based on NSGA-II

Based on the fatigue load and platform motion modeling of the semi-submersible wind turbine, this section proposes a multi-objective optimization method based on the NSGA-II algorithm to reduce fatigue loads while optimizing platform motion. When designing the semi-submersible wind turbine, the fatigue load and platform motion could be the primary and secondary concerns for designers. The relation between the fatigue load and platform motion is nonlinear and complicated, and a trade-off between fatigue load and platform motion is necessary to make. In this context, multi-objective optimization provides more freedoms for the designers to select, meeting their requirements.

4.2.1. Objective Functions

(1) Objective Function for Fatigue Load Optimization

The fatigue load optimization of key components in the semi-submersible wind turbine, namely the blade root, tower base, drivetrain, and mooring lines, aims to reduce fatigue damage caused by environmental loads over long-term operation and improve the reliability and lifespan of the turbine structure. The objective function is set as the following:

$$f_{DEL} = \sum_{i=1}^{M} w_i DEL_i \cdot \left(\frac{\left| DEL_i - DEL_{ref} \right|}{DEL_{ref}} \right) \quad (5)$$

where DEL_i is the DEL of the i component; DEL_{ref} is the reference DEL value; w_i is the weight coefficient for the component; M is the total number of components.

During optimization, the weight coefficient w_i can be adjusted based on the importance of different components. Since the DELs of the blade root and tower base have a significant impact on the overall safety of the semi-submersible wind turbine, they are given higher weights, set as 0.35. The DELs of the drivetrain and mooring lines have lower weights, set as 0.1 and 0.2, respectively. It is worth noting that the fatigue damage for each component may vary under different operating conditions, so a balance must be made based on actual conditions during optimization.

(2) Objective Function for Platform Motion Optimization

The platform motion optimization of the semi-submersible wind turbine focuses on minimizing the maximum horizontal displacement S_{max} of the platform to reduce excessive dynamic loads caused by wind and waves and prevent excessive motion from negatively affecting the turbine. The objective function is set as the following:

$$f_{s_{max}} = w_X \cdot X_{max}^2 + w_Y \cdot Y_{max}^2 \tag{6}$$

where ΔX_{max} and ΔY_{max} are the maximum displacements of the platform in the X and Y directions; w_X and w_Y are the weight coefficients for each direction. In this study, w_X and w_Y are equal to 0.5.

During optimization, the horizontal motion characteristics of the platform should be considered. For instance, under certain wind and wave conditions, the X-direction motion may be more prominent, in which case w_X can be increased to reduce motion in that direction. However, excessive suppression of platform motion may lead to unreasonable control strategies. For example, excessive yaw angle adjustments may affect power output, so optimization must balance reducing platform motion and maintaining stable turbine operation.

4.2.2. Constraints

To ensure the reasonableness of the optimization results, several constraints are set:

(1) Control Constraints: The minimum and maximum ranges for yaw angle, pitch angle, generator speed, and power must be respected.

$$\theta_{yaw,min} \leq \theta_{yaw}(t) \leq \theta_{yaw,max} \tag{7}$$

$$\theta_{pitch,min} \leq \theta_{pitch}(t) \leq \theta_{pitch,max} \tag{8}$$

$$w_{gen,min} \leq w_{gen}(t) \leq w_{gen,max} \tag{9}$$

$$P_{gen,min} \leq P_{gen}(t) \leq P_{gen,max} \tag{10}$$

(2) Platform Motion Constraints: The maximum displacement values of the platform must be limited.

$$\Delta x(t) \leq \Delta x_{max} \tag{11}$$

$$\Delta y(t) \leq \Delta y_{max} \tag{12}$$

These constraints ensure that the control parameters for the servos and the platform's motion remain within reasonable physical limits during the optimization process.

4.2.3. NSGA-II Multi-Objective Optimization Algorithm

NSGA-II (Non-dominated Sorting Genetic Algorithm II) is an improved multi-objective genetic algorithm that uses non-dominated sorting and crowding distance strategies to maintain solution diversity, making it effective for solving complex multi-objective optimization problems [32].

(1) Non-Dominated Sorting: Individuals are sorted based on their dominance relationships, maintaining diversity and preventing premature convergence.
(2) Crowding Distance: The crowding distance measures the distribution of the solution set. Individuals with larger crowding distances are prioritized, ensuring diversity while avoiding premature convergence.

The NSGA-II solution process is as follows: First, the algorithm initializes a population of size population_size, where each individual represents a potential solution. The population is subjected to fast non-dominated sorting, dividing the individuals into different Pareto fronts. For each front, the crowding distance of the individuals is calculated to assess the distribution of solutions. Next, the algorithm generates a new offspring by selecting two parents from the current population using tournament selection, performing crossover to generate two offspring, and applying mutation. This process continues until the offspring population reaches population_size. The parent and offspring populations are merged into a combined population, and fast non-dominated sorting is performed again. The algorithm selects individuals from each Pareto front to form a new population, filling the population_size. If the number of individuals in a front exceeds the available space, individuals are sorted by crowding distance, and the best individuals are selected. Finally, the new population replaces the original population and enters the next iteration of optimization.

4.2.4. Pareto Optimal Solution Evaluation Metrics

In multi-objective optimization, there are typically conflicts and competition between objective functions, so a solution cannot achieve optimal results in all objectives simultaneously. A Pareto optimal solution is one where no other solution can improve on one objective without worsening another. To evaluate the quality of the Pareto optimal solution set, several metrics are used to ensure that the optimization process finds solutions that are both diverse and widely spread across the objective space. The following three key evaluation metrics are adopted:

(1) Crowding Distance: The crowding distance measures the "crowdedness" of a solution in the objective space. For each solution in the set, its crowding distance is calculated as follows:

$$d_i = \sum_{m=1}^{M} \left(\frac{f_m(i+1) - f_m(i-1)}{f_m^{max} - f_m^{min}} \right) \tag{13}$$

where $f_m(i)$ is the objective value of solution i for objective m; f_m^{max} and f_m^{min} are the maximum and minimum objective values for objective m in the solution set; $i+1$ and $i-1$ are the adjacent solutions in the direction of objective m. The larger the crowding distance, the fewer solutions exist in the neighborhood, helping to maintain diversity in the solution set.

(2) Hypervolume Indicator: The hypervolume measures the volume of the objective space covered by the solution set. Given a reference point $R = (\gamma_1, \gamma_2, \cdots, \gamma_M)$, the hypervolume $HV(S)$ is defined as the volume covered by the union of solutions in S:

$$HV(S) = Vol(\cup_{i \in S}[\gamma, f(x_i)]) \tag{14}$$

where S is the solution set, x_i is the i solution in the set, $f(x_i)$ is the objective vector for x_i, and $[\gamma, f(x_i)]$ is the volume between the reference point γ and the objective vector $f(x_i)$. The larger the hypervolume, the better the optimization result.

(3) Solution Set Diversity: The diversity of the solution set is a measure of the uniformity of its distribution in the objective space. A common diversity metric is the average distance or standard deviation between solutions in the set. The diversity of a set of NNN solutions $x_1, x_2, \cdots, x_N$ can be measured as follows:

$$D(S) = \frac{1}{N} \sum_{i=1}^{N} \sum_{j=i+1}^{N} d(x_i, x_j) \tag{15}$$

where $d(x_i, x_j)$ is the Euclidean distance between solutions x_i and x_j, and N is the number of solutions in the set. A higher diversity indicates a broader coverage of the objective space.

5. Case Study in Actual Marine Environment

To demonstrate the practical relevance of the proposed approach, a case study is conducted using environmental data from the East China Sea. This case is selected because it provides realistic wind–wave conditions representative of actual offshore operation. By applying the data-driven surrogate model and multi-objective optimization framework to these conditions, the case study validates the effectiveness of the method in reducing component fatigue loads and platform motion under realistic marine environments, thereby confirming its potential applicability for real offshore wind turbine operations.

5.1. Simulation Setup

The simulation environment is set up based on marine and meteorological observation data from 2018 to 2022 at the Lianyungang Marine Observation Station in the East China Sea. The data is sourced from the China National Science and Technology Resources Sharing Service Platform (http://mds.nmdis.org.cn/), covering key factors such as wind speed, wave height, and ocean current. The wind speed ranges from 3 to 25 m/s, wave height ranges from 0 to 3 m, wave period ranges from 0 to 15 s, wind direction ranges from 0 to 360°, and ocean current speed is 0.5 m/s.

In terms of control, three main servo systems are used: yaw control, pitch control, and generator speed control. Yaw control ensures that the wind turbine yaw motion stays within constraints; pitch control adjusts the blade pitch angle automatically according to wind speed variations to prevent overloading; generator speed is adjusted based on wind speed to keep it within the rated power output range. The constraint ranges for the control quantities of the three servo mechanisms are set as shown in Table 6.

Table 6. Constraint range settings for servo mechanism control variables.

Control Variable	Constraint Range
Yaw Angle	$-30^\circ \leq \varphi_{gset} \leq 30^\circ$
Pitch Angle	$0^\circ \leq \beta_{gset} \leq 10^\circ$
Generator Speed	973 rpm $\leq \omega_{gset} \leq$ 1173 rpm

After setting the semi-submersible wind turbine, environmental parameters, and servo mechanism control constraints, the NSGA-II algorithm is used to adjust the control quantities of the servo mechanisms to optimize fatigue loads and platform responses. The objective functions include fatigue load suppression and platform motion optimization, aiming to reduce both fatigue damage to the components and dynamic motion responses of the platform. The input parameters for the NSGA-II algorithm are set as shown in Table 7.

Table 7. Parameter settings of the NSGA-II algorithm.

Algorithm Input Parameters	Value
Population Size	100
Maximum Iterations	200
Crossover Probability	0.8
Mutation Probability	0.02

5.2. Optimization Results and Discussion

Before optimization, the settings and results of the original scheme (R_0) are shown in Table 8. The yaw angle is 10°, pitch angle is 7°, generator speed is 1071 rpm, wind speed is 13 m/s, wave height is 0.1 m, wave period is 5 s, and wind direction is 296°. Based on the simulation results, the DELs for the tower base, blade root, drivetrain, and mooring lines in scheme R_0 are 5705.937, 5817.089, 4143.517, and 16,453.31, respectively. The platform's S_{max} is 12.740 m. Although the scheme meets design conditions, it fails to find a better balance between fatigue load and platform motion. On one hand, the DEL values for scheme R_0 are high, indicating large fatigue loads on key components. High fatigue loads not only shorten the service life of key components but may also increase maintenance costs and downtime. On the other hand, the platform's S_{max} is large, indicating significant platform motion during operation. Excessive horizontal displacement increases platform motion, affecting turbine stability and power generation efficiency, and could even lead to platform tilting or instability under extreme conditions. Therefore, scheme R_0 may face significant platform motion and high fatigue loads in practical operation, negatively impacting turbine performance and reliability and reducing feasibility. Optimization of scheme R_0 is necessary.

Table 8. Model settings and results of the R_0 scheme simulation.

Parameter	Value
Wind Speed (m/s)	13 m/s
Wave Height (m)	0.1 m
Wave Period (s)	5 s
Wind Direction (°)	296°
Yaw Angle (°)	10°
Pitch Angle (°)	7°
Generator Speed (rpm)	1071 rpm
Tower Base DEL	5705.937
Blade Root DEL	5817.089
Drivetrain DEL	4143.517
Mooring Lines DEL	16,453.31
Platform S_{max}	12.740 m

The Pareto front results for the optimized key component DELs and platform S_{max} are shown in Figure 9. The points in the figure represent different optimization solutions, with each point showing a balance between multiple objectives. The Pareto front forms a boundary, and any solution on this front cannot be further optimized. That is, any improvement in one objective will result in a deterioration of another. By inspecting the Pareto front, we observe that the total DEL for the semi-submersible wind turbine key components decreases as S_{max} increases. The minimum total DEL for the key components is approximately 27,611, with a corresponding S_{max} of about 11.52 m. Therefore, this is the optimal solution for key component DEL optimization, rather than the optimal solution for platform S_{max} optimization. No solution exists that can simultaneously minimize both the total DEL of key components and the platform S_{max}.

On the Pareto front, eight optimization solutions (R_1, R_2, R_3, R_4, R_5, R_6, R_7, R_8) are selected to evaluate the most suitable solution. The analysis results of the crowding degree, hypervolume, and diversity of these eight solutions are shown in Table 9.

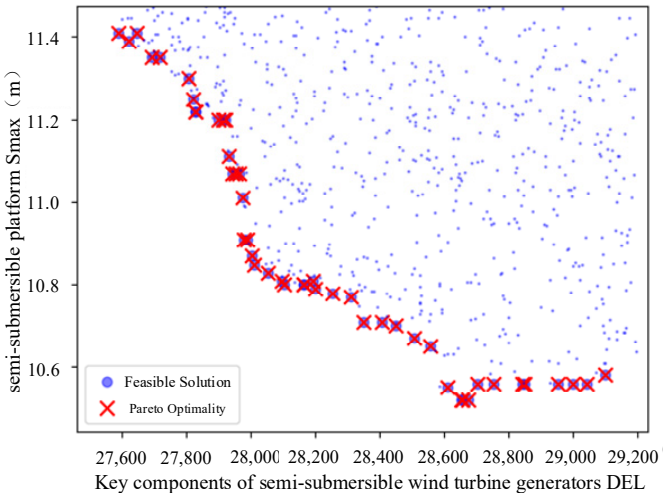


Figure 9. Pareto frontier for the comprehensive optimization of target component DEL and platform S_{max}.

Table 9. Calculation results of evaluation indicators for the eight solutions.

Solution Set	Crowding Degree	Hypervolume	Diversity
R_1 = [29,100.76, 10.58]	∞	5100	450
R_2 = [27,589.29, 11.41]	∞	5100	450
R_3 = [27,831.08, 11.22]	480	5100	380
R_4 = [28,165.26, 10.80]	300	5100	400
R_5 = [28,254.02, 10.78]	350	5100	430
R_6 = [28,450.76, 10.70]	370	5100	420
R_7 = [28,658.17, 10.59]	300	5100	410
R_8 = [28,840.89, 10.59]	320	5100	415

From Table 9, the boundary solutions (R_1 and R_2) have a crowding degree of ∞, indicating that they are at the extremes of the Pareto front, occupying the extreme positions in the objective space and having a significant influence. In contrast, the internal solutions (R_3, R_4, R_5, R_6, R_7, R_8) have smaller crowding degrees, showing that they are evenly distributed in the objective space without noticeable repetition or overcrowding. Most of the solutions have crowding degrees between 300 and 480, indicating a uniform distribution with no significant concentration. This distribution helps ensure solution diversity and avoids local optima. All selected solutions have a hypervolume of 5100, meaning they cover a large region of the objective space. A larger hypervolume typically indicates better global exploration capabilities. The diversity values for the solutions are between 400 and 450, showing a good distribution in the objective space, and the optimization process effectively avoids local concentration. In summary, the selected eight solutions demonstrated good characteristics in terms of evaluation metrics such as crowding degree, hypervolume, and diversity. These solutions not only exhibited a relatively even distribution in the objective space but also performed excellently in terms of coverage and diversity. Therefore, these solutions are considered the optimal feasible solutions in this optimization process and are suitable for further optimization analysis.

The optimization results for the eight schemes (R_1, R_2, R_3, R_4, R_5, R_6, R_7, R_8) are shown in Table 10. As seen from the table, the total DEL and platform S_{max} of the eight schemes are all smaller than those of the pre-optimization scheme (R_0), indicating that the proposed optimization method has greatly improved the total DEL of the key components and the platform S_{max} of the semi-submersible wind turbine. For the optimization of the total DEL of the key components, scheme R_2 is the best solution. The optimized total DEL in scheme R_2 is the smallest at 27,589.29, representing a reduction

of approximately 14.1% compared to the original R_0 scheme, with a significant decrease in fatigue load. On the other hand, scheme R_1 results in the largest total DEL after optimization, with a reduction of approximately 9.3% compared to the original R_0 scheme. For the optimization of platform S_{max}, scheme R_1 is the best. The optimized S_{max} in R_1 is the smallest at 10.58 m, representing a reduction of approximately 16.95% compared to the original R_0 scheme. Therefore, the optimization effect on platform motion for these eight schemes is less significant than the improvement in fatigue load. However, these optimization results are meaningful, as it shows that the platform motion is optimizable by using the presented scheme. The platform motion, serving as an indirect indicator of performance, unlike fatigue loads, is primarily determined by the mooring system. More reduction on platform motion can be fulfilled by simultaneously optimizing the mooring system and the control system.

Table 10. Optimization results of the eight schemes.

Scheme	Yaw Angle (°)	Pitch Angle (°)	Generator Speed (rpm)	Total DEL	S_{max} (m)
R_0	10	7	1071	32,119.853	12.740
R_1	10.13	2.61	1166.52	29,100.76	10.58
R_2	12.11	1.54	1142.80	27,589.29	11.41
R_3	20.21	4.72	1181.00	27,831.08	11.22
R_4	22.87	1.89	1162.29	28,165.26	10.80
R_5	11.30	2.45	1156.92	28,254.02	10.78
R_6	21.04	5.75	1128.29	28,450.76	10.76
R_7	17.16	3.02	1131.96	28,658.17	10.59
R_8	21.05	6.96	1121.65	28,840.89	10.59

In summary, by adjusting the yaw angle, pitch angle, and generator speed, the fatigue loads on the key components of the semi-submersible wind turbine are effectively reduced, with only slight changes in platform motion. The optimized S_{max} ranged from 10.6 m to 11.4 m, and while all optimization schemes reduced horizontal displacement to some degree, none outperformed scheme R_1 significantly. From the analysis in Section 3 on the impact of different control variables on fatigue load and platform motion, it is clear that the mooring system's fatigue load is the highest among the four key components, and platform motion has a substantial impact on it. Therefore, scheme R_1 is the optimal choice among the eight schemes.

Although scheme R_2 did not optimize S_{max} as well as R_1, it achieved the greatest reduction in DEL, making it suitable for scenarios with a higher emphasis on fatigue load reduction. The optimization effects of other schemes were relatively modest, with some improvement in DEL, but minimal changes in horizontal displacement.

Figure 10 shows the radar chart for the key components' DELs (tower base DEL, blade root DEL, drivetrain DEL, mooring lines DEL) and platform S_{max} under schemes R_0 and R_1. This comparison provides a clear visualization of the changes in the key indicators before and after optimization. As seen in Figure 10, the total DEL of the R_0 scheme is clearly higher than that of the R_1 scheme. This indicates that under the original R_0 scheme, the fatigue load on each component of the semi-submersible wind turbine is relatively large. In particular, the DEL values for key components such as the tower base DEL, blade root DEL, and mooring lines DEL are higher, implying that these components experience a greater accumulation of fatigue loads, which may lead to higher maintenance frequencies and shorter service lives. However, in the optimized R_1 scheme, in addition to the reduction in total DEL, another notable change is the reduction in the DEL of the tower base, blade root, drivetrain, and mooring lines compared to R_0. Notably, the mooring

lines DEL experienced a significant reduction. Therefore, the proposed optimization method not only achieved a significant reduction in total DEL but also reduced the fatigue load on the key components, with remarkable optimization results. This makes it more advantageous in practical applications. Furthermore, platform S_{max} was also optimized in scheme R_1, reducing from 12.74 m in R_0 to 10.58 m. Overall, the optimization method significantly reduces the fatigue loads of the four key components and decreased platform motion, improving the stability of the semi-submersible wind turbine in wind and wave environments. More advanced optimization can be referred to [33,34].

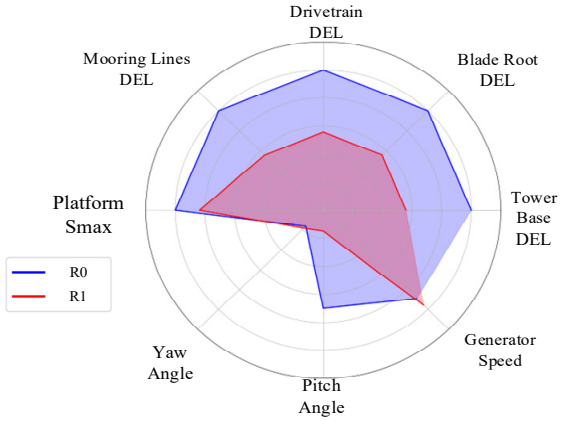


Figure 10. Radar chart of DEL of key components and platform horizontal displacement of the Semi-submersible wind turbine under R_0 and R_1.

Although this study focuses on a specific set of environmental conditions derived from the East China Sea, it is important to acknowledge that the generalizability of the findings to other sea states remains uncertain. The decision to limit the case study to this particular marine environment was made to avoid redundancy and ensure a focused evaluation of the proposed method. However, the method's applicability to different sea states, with varying wind speeds, wave heights, and current conditions, remains a subject for future research. Testing across a broader range of sea states would provide a more comprehensive validation of the approach and further confirm its robustness under different operational scenarios.

6. Conclusions

This study focuses on the load suppression and platform motion optimization of semi-submersible wind turbines, combining theoretical analysis, data-driven modeling, and multi-objective optimization methods. The influence of control variables on the DEL of key components and the Smax of the platform is systematically explored, and the effectiveness of the optimization strategy is verified. The main conclusions are as follows:

(1) Significant influence of generator speed and yaw angle on fatigue load and platform motion: Increasing the generator speed increases the fatigue loads on the blade root and drivetrain, changing the force distribution on the mooring lines. Increasing the yaw angle enlarges the platform motion range, with positive and negative yaw having a symmetrical effect on the blade root and tower base loads. Active power has a small effect on mooring line loads but is sensitive to blade root and tower base loads.

(2) Feasibility and effectiveness of data-driven modeling and multi-objective optimization strategy: The random forest (RF) model provides the highest accuracy in fatigue load prediction (with overall error < 0.05). The Pareto frontier obtained by combining the NSGA-II algorithm allows for the coordinated optimization of fatigue load and platform motion.

(3) Case studies show that the total DEL for key components can be reduced by up to 14.1%, and platform Smax can be reduced by up to 16.95%, significantly improving the structural safety and operational stability of the wind turbine.

This study offers a new approach for optimizing the entire life cycle of semi-submersible wind turbines and provides a reference for the engineering application of floating wind turbine technology in complex marine environments. By systematically quantifying the coupled effects of generator speed, pitch, and yaw on turbine performance, the results provide valuable references for the design of next-generation floating turbines with improved load resilience and motion suppression capabilities. In addition, the integration of machine learning-based surrogate models into optimization demonstrates a practical pathway for developing advanced control systems that can operate in real time and adapt to site-specific marine conditions. Furthermore, the approach highlights the potential to bridge structural health monitoring, control optimization, and turbine design, thereby contributing to the long-term reliability and cost-effectiveness of offshore wind energy. This study is mainly conducted with simulations, and future research could be launching experimental campaigns.

Author Contributions: Conceptualization, D.S.; Methodology, L.L., L.W. and L.H.; Software, Q.H. and S.C.; Validation, Q.H.; Investigation, L.L. and J.Y.; Resources, J.Y.; Data curation, L.L. and L.H.; Writing—original draft, Q.H., L.W. and D.S.; Visualization, L.W. All authors have read and agreed to the published version of the manuscript.

Funding: This research is supported by the Natural Science Foundation of Hunan Province (2021JJ30875), the science and technology innovation Program of Hunan Province (2023RC3174), the Natural Science Foundation of Changsha (kq2208288), the SKL—OWPE & WEHEU under Grants (HFQZ2025-03).

Data Availability Statement: The original contributions presented in this study are included in the article. Further inquiries can be directed to the corresponding author.

Conflicts of Interest: Sifan Cheng was employed by Mingyang Smart Energy Group Co., Ltd. The remaining authors declare that the research was conducted in the absence of any commercial or financial relationships that could be construed as a potential conflict of interest.

References

1. Global Wind Energy Council. *Global Wind Report 2023*; Global Wind Energy Council (GWEC): Lisbon, Portugal, 2023.
2. Jonkman, J.; Matha, D. *Quantitative Comparison of the Responses of Three Floating Platforms*; National Renewable Energy Lab. (NREL): Golden, CO, USA, 2010.
3. Jacobsen, A.; Godvik, M. Influence of wakes and atmospheric stability on the floater responses of the Hywind Scotland wind turbines. *Wind Energy* **2021**, *24*, 149–161. [CrossRef]
4. Ozmutlu, S. Mooring System Supply and Anchor Design for WindFloat Atlantic Project. In Proceedings of the Offshore Technology Conference, Houston, TX, USA, 1 May 2022.
5. Zou, Q.; Lu, Z.; Shen, Y. Short-term prediction of hydrodynamic response of a novel semi-submersible FOWT platform under wind, current and wave loads. *Ocean Eng.* **2023**, *278*, 114471. [CrossRef]
6. Bai, D.; Wang, B.; Li, Y.; Wang, W. Study on load reduction and vibration control strategies for semi-submersible offshore wind turbines. *Sci. Rep.* **2025**, *15*, 1148. [CrossRef] [PubMed]
7. Li, Q.; Kamada, Y.; Maeda, T.; Murata, J.; Iida, K.; Okumura, Y. Fundamental study on aerodynamic force of floating offshore wind turbine with cyclic pitch mechanism. *Energy* **2016**, *99*, 20–31. [CrossRef]
8. Gong, Y.; Yang, Q.; Geng, H.; Wang, L. Dynamic Modeling and Control for an Offshore Semi-submersible Floating Wind Turbine. *IEEE Trans. Autom. Sci. Eng.* **2025**, *22*, 12371–12382. [CrossRef]
9. Han, C.; Homer, J.R.; Nagamune, R. Movable range and position control of an offshore wind turbine with a semi-submersible floating platform. In Proceedings of the 2017 American Control Conference (ACC), Seattle, WA, USA, 24–26 May 2017; pp. 1389–1394.
10. Qi, L.; Wu, H.; Guo, N.; Cai, C.; Zhou, T.; Shi, K.; Zhong, X.; Xu, J. Regulating rotor aerodynamics and platform motions for a semi-submersible floating wind turbine with trailing edge flaps. *Ocean Eng.* **2023**, *286*, 115629. [CrossRef]

11. Stewart, G.; Lackner, M. Offshore wind turbine load reduction employing optimal passive tuned mass damping systems. *IEEE Trans. Control Syst. Technol.* **2013**, *21*, 1090–1104. [CrossRef]
12. Xie, J.; Dong, H.; Zhao, X. Power regulation and load mitigation of floating wind turbines via reinforcement learning. *IEEE Trans. Autom. Sci. Eng.* **2023**, *21*, 4328–4339. [CrossRef]
13. Lara, M.; Vázquez, F.; Sandua-Fernández, I.; Garrido, J. Adaptive Active Generator Torque Controller Design Using Multi-Objective Optimization for Tower Lateral Load Reduction in Monopile Offshore Wind Turbines. *IEEE Access* **2023**, *11*, 115894–115910. [CrossRef]
14. Zhou, S.; Li, C.; Xiao, Y.; Wang, X.; Xiang, W.; Sun, Q. Evaluation of floating wind turbine substructure designs by using long-term dynamic optimization. *Appl. Energy* **2023**, *352*, 121941. [CrossRef]
15. Civera, M.; Surace, C. Non-Destructive Techniques for the Condition and Structural Health Monitoring of Wind Turbines: A Literature Review of the Last 20 Years. *Sensors* **2022**, *22*, 1627. [CrossRef] [PubMed]
16. Kuai, H.; Civera, M.; Coletta, G.; Chiaia, B.; Surace, C. Cointegration strategy for damage assessment of offshore platforms subject to wind and wave forces. *Ocean Eng.* **2024**, *304*, 17. [CrossRef]
17. Roddier, D.; Cermelli, C.; Aubault, A.; Weinstein, A. WindFloat: A floating foundation for offshore wind turbines. *J. Renew. Sustain. Energy* **2010**, *2*, 033104. [CrossRef]
18. Jonkman, B.J. *TurbSim User's Guide*; National Renewable Energy Lab. (NREL): Golden, CO, USA, 2006.
19. Li, Z.; Yan, Y.; Li, C.; Minnan, Y.U.; Shicheng, X.U. Analysis of Dynamic Response and Structural Damage of Large-scale Wind Turbine Under Combined Action of Wind-Wave-Earthquake with Gravity Load. *J. Chin. Soc. Power Eng.* **2022**, *42*, 753–761.
20. Kanellos, F.D.; Hatziargyriou, N.D. Control of variable speed wind turbines in islanded mode of operation. *IEEE Trans. Energy Convers.* **2008**, *23*, 535–543. [CrossRef]
21. Chen, J.; Jin, C.; Kim, M.H. Systematic comparisons among OpenFAST, Charm3D-FAST simulations and DeepCWind model test for 5 MW OC4 semisubmersible offshore wind turbine. *Ocean Syst. Eng.* **2023**, *13*, 173–193.
22. Zhao, H.; Wu, Q.; Huang, S.; Shahidehpour, M.; Guo, Q.; Sun, H. Fatigue load sensitivity-based optimal active power dispatch for wind farms. *IEEE Trans. Sustain. Energy* **2017**, *8*, 1247–1259. [CrossRef]
23. Sun, J.; Chen, Z.; Yu, H.; Gao, S.; Wang, B.; Ying, Y.; Sun, Y.; Qian, P.; Zhang, D.; Si, Y. Quantitative evaluation of yaw-misalignment and aerodynamic wake induced fatigue loads of offshore Wind turbines. *Renew. Energy* **2022**, *199*, 71–86. [CrossRef]
24. He, R.; Yang, H.; Lu, L. Optimal yaw strategy and fatigue analysis of wind turbines under the combined effects of wake and yaw control. *Appl. Energy* **2023**, *337*, 120878. [CrossRef]
25. Navarrete, E.C.; Perea, M.T.; Correa, J.J.; Serrano, R.C.; Ríos-Moreno, G. Expert control systems implemented in a pitch control of wind turbine: A review. *IEEE Access* **2019**, *7*, 13241–13259. [CrossRef]
26. Xing, Z.; Chen, L.; Sun, H.; Zhe, W. Strategies study of individual variable pitch control. *Proc. CSEE* **2011**, *31*, 131–138.
27. Xiao, Y.; Wang, X.; Sun, X.; Zhong, X.; Peng, C.; Dai, L.; Maeda, T.; Cai, C.; Li, Q. Load reduction and mechanism analysis of cyclic pitch regulation on wind turbine blades under yaw conditions. *Ocean Eng.* **2025**, *321*, 120361. [CrossRef]
28. Jian, Y.; Songyue, Z.; Dongran, S.; Su, M.; Yang, X.; Joo, Y.H. Data-driven modelling for fatigue loads of large-scale wind turbines under active power regulation. *Wind Energy* **2021**, *24*, 558–572.
29. Jeon, T.; Kim, B.-S.; Kim, J.; Paek, I.; Lim, C.-H. Parametric Analysis of Control Techniques for 15 MW Semi-Submersible Floating Wind Turbine. *Appl. Sci.* **2025**, *15*, 519. [CrossRef]
30. Yuan, X.; Song, D.; Chen, S.; Yang, J.; Dong, M.; Wei, R.; Chen, S.; Talaat, M.; Joo, Y.H. Deep analysis of power regulation on fatigue loads and platform motion in floating wind turbines. *Ocean Eng.* **2024**, *313*, 119667. [CrossRef]
31. Yuan, X.; Huang, Q.; Song, D.; Xia, E.; Xiao, Z.; Yang, J.; Dong, M.; Wei, R.; Evgeny, S.; Joo, Y. Fatigue Load Modeling of Floating Wind Turbines Based on Vine Copula Theory and Machine Learning. *J. Mar. Sci. Eng.* **2024**, *12*, 1275. [CrossRef]
32. Wang, Q.; Li, Z. Multi-objective transmission planning associated with wind farms applying NSGA-II hybrid intelligent algorithm. *Proc. CSEE* **2011**, *31*, 17–24.
33. Wang, Y.; Song, D.; Jurić, F.; Duić, N.; Mikulčić, H. Multi-modal optimization of offshore wind farm collection system topology based on nearest better most attractive particle swarm optimization. *Renew. Sustain. Energy Rev.* **2025**, *222*, 115978. [CrossRef]
34. Huang, C.; Wang, L.; Huang, Q.; Song, D.; Yang, J.; Dong, M.; Dui, N. Bi-level multi-objective optimization framework for wake escape in floating offshore wind farm. *Appl. Energy* **2025**, *377*, 124712. [CrossRef]

Disclaimer/Publisher's Note: The statements, opinions and data contained in all publications are solely those of the individual author(s) and contributor(s) and not of MDPI and/or the editor(s). MDPI and/or the editor(s) disclaim responsibility for any injury to people or property resulting from any ideas, methods, instructions or products referred to in the content.